



## A Search for SM Higgs boson using the $ZH \rightarrow \nu\bar{\nu}b\bar{b}$ channel in $p\bar{p}$ Collisions at $\sqrt{s} = 1.96$ TeV

The DØ Collaboration  
URL: <http://www-d0.fnal.gov>  
(Dated: April 14, 2005)

This note describes a search for the standard model Higgs boson produced in association with the  $Z$  boson at DØ, based on an integrated luminosity of  $L=261 \text{ pb}^{-1}$  of data. We study the  $p\bar{p} \rightarrow ZH \rightarrow \nu\bar{\nu}b\bar{b}$  channel, which is one of the most sensitive ways to search for light Higgs bosons because of the large  $Z \rightarrow \nu\bar{\nu}$  and  $H \rightarrow b\bar{b}$  branching ratios. The analysis starts with a sample of multijet events with large imbalance in transverse momentum. We then select events with two  $b$ -tagged jets and search for a peak in their invariant mass distribution. After subtracting the backgrounds, we measure the 95 % C.L. upper limits on the  $\sigma(p\bar{p} \rightarrow ZH) \times Br(H \rightarrow b\bar{b})$  for Higgs masses between 105 and 135 GeV to be 7.7–12.2 pb.

*Preliminary Results for Winter 2005 Conferences*

## I. INTRODUCTION

The Higgs boson is the only particle in the standard model that has not been directly observed. Since the Higgs boson plays a crucial role in the mechanism of electroweak symmetry breaking, it is important to search for it at the Tevatron. LEP experiments provide lower limits on its mass, and electroweak global fits favor a relatively light Higgs boson. Tevatron Run II experiments have the capability to observe a Higgs boson of low mass. Thus, a search for the Higgs boson is one of the most important goals of the DØ and CDF experiments [1],[2].

The  $p\bar{p} \rightarrow ZH \rightarrow \nu\bar{\nu}b\bar{b}$  channel is one of the most sensitive ways to search for a light Higgs boson because of the large  $Z \rightarrow \nu\bar{\nu}$  and  $H \rightarrow b\bar{b}$  branching ratios. The product of cross section and branching fraction is expected to be about 0.01 pb for a light Higgs boson, which is almost as large as that of  $WH \rightarrow l\nu b\bar{b}$  [3].

The final state has two  $b$  jets from Higgs boson decay, and missing  $E_T$  ( $\cancel{E}_T$ ) due to the two neutrinos from  $Z$  decay. The two  $b$  jets are boosted along the Higgs momentum direction. Therefore, they tend to be acoplanar in contrast to typical back-to-back QCD dijet production. There are two main sources of the background to this channel. The physics backgrounds are  $Z$ +jets,  $W$ +jets, electroweak diboson production like  $WZ$  and  $ZZ$  production, and top quark production with escaping leptons or jets. On the other hand, the instrumental background is caused by multijet events with mismeasurement of the jet energy or misidentification of jets. Selecting events with large missing transverse energy and two  $b$ -tagged jets rejects a large fraction of multijet background. Since trigger and selection criteria rely on jets, good understanding of the calorimeter response and  $b$ -tagging are the main ingredients of this analysis.

## II. DATA SAMPLE AND EVENT SELECTION

The DØ detector has a magnetic central-tracking system surrounded by an uranium/liquid-argon calorimeter, which is contained within a muon spectrometer. The central-tracking system consists of a silicon microstrip tracker (SMT) and a central fiber tracker (CFT), both located within a 2 T superconducting solenoidal magnet [4]. The SMT and CFT have designs optimized for tracking and vertexing capabilities for pseudorapidities  $|\eta| < 3$  and 2.5, respectively. The calorimeter has a central section (CC) covering up to  $|\eta| \approx 1.1$ , and two end calorimeters (EC) extending coverage to  $|\eta| \approx 4.2$ , all housed in separate cryostats [5]. For particle identification, the calorimeter is divided into an electromagnetic (EM) part followed by fine (FH) and coarse (CH) hadronic sections. Scintillators between the CC and EC cryostats provide additional sampling of developing showers for  $1.1 < |\eta| < 1.4$ . The muon system resides beyond the calorimeter, and consists of a layer of tracking detectors and scintillation trigger counters in front of 1.8 T toroids, followed by two similar layers behind the toroids which provide muon tracking for  $|\eta| < 2$ . The luminosity is measured using scintillator arrays located in front of the EC cryostats, covering  $2.7 < |\eta| < 4.4$ .

A dedicated trigger has been designed to select events with acoplanar jets accompanied by  $\cancel{E}_T$  from March 2003 to June 2004. The integrated luminosity is  $261 \text{ pb}^{-1}$  after the requirement of good data quality. The event selection requires at least two jets with  $p_T > 20 \text{ GeV}$  in  $|\eta| < 2.5$ . Jets are required to pass quality cuts to reject noise and electromagnetic objects and their energies are corrected back to the particle level for detector and physics effects using the standard jet energy scale factors. The correction depends on the  $p_T$  and  $\eta$  of jets and is typically 30 % for the data and 20 % for the simulation. The jet resolution is measured by energy balance of the jet+ $\gamma$  process and is typically 10 – 15 % for data and 6 – 10 % for the simulation. The difference between data and simulation is taken into account by smearing the jets in simulation.

The requirements of  $\cancel{E}_T > 25 \text{ GeV}$ , no back-to-back event topology, and no isolated tracks in the event reject QCD multijet,  $W(\rightarrow e\nu, \mu\nu)$ +jet, and  $Z(\rightarrow ee, \mu\mu)$ +jet events.  $H_T$ , the scalar sum of the jet  $p_T$ , is required to be less than 200 GeV for the rejection of  $t\bar{t}$  background. To further reduce the background, we define the following variables:

- $\min\Delta\phi(\cancel{E}_T, \text{jets})$  :  
the minimum of the difference in azimuthal angle  $\phi$  between the direction of  $\cancel{E}_T$  and any of the jets
- $\cancel{H}_T \equiv |\sum_i^{n_{jet}} \vec{p}_T|$  :  
the magnitude of the vector sum of accepted jet  $p_T$
- $P_T^{trk} \equiv |\sum_i^{n_{trk}} \vec{p}_T|$  :  
the magnitude of the vector sum of all tracks'  $p_T$
- $P_{T,2}^{trk} \equiv |\sum_i^{n_{trk} \text{ in dijet}} \vec{p}_T|$  :  
the magnitude of the vector sum of the  $p_T$  of the tracks within the cones of  $\Delta R = \sqrt{(\Delta\eta)^2 + (\Delta\phi)^2} < 0.5$  of the two leading jets.

- $\text{Asym}(\cancel{E}_T, \cancel{H}_T) \equiv (\cancel{E}_T - \cancel{H}_T) / (\cancel{E}_T + \cancel{H}_T)$
- $R_{P_T^{trk}} \equiv (P_T^{trk} - P_{T,2}^{trk}) / P_T^{trk}$

The instrumental background is significantly reduced by requiring:  $\cancel{E}_T / \text{GeV} > -40 \times \min\Delta\phi(\cancel{E}_T, \text{jet}) + 80$ ,  $P_T^{trk} > 20 \text{ GeV}$ ,  $0 < (\cancel{E}_T - P_T^{trk}) / (\cancel{E}_T + P_T^{trk}) < 0.6$ , and  $-0.1 < \text{Asym}(\cancel{E}_T, \cancel{H}_T) < 0.2$ .

The variables listed above are studied in  $W$ +jets samples to assure they are well modeled. The comparison of  $\text{Asym}(\cancel{E}_T, \cancel{H}_T)$  and  $R_{P_T^{trk}}$  in  $W$ +jets data with simulation are shown in FIG.1. As discussed in section IV, the signal region is defined as  $|R_{P_T^{trk}}| < 0.2$ , and the sideband defined as  $0.3 < |R_{P_T^{trk}}| < 1.0$  is used to measure the instrumental background shape. FIG.2. shows the scatter plots of  $\text{Asym}(\cancel{E}_T, \cancel{H}_T)$  and  $R_{P_T^{trk}}$  for data, signal simulation, physics background simulation, and instrumental simulation. The signal and sideband regions are also shown in these figures. The signal and physics simulations have a peak in the signal region, while there is no peak in the instrumental background simulation.

It is difficult to tell a  $b$ -jet from a light quark jet if it does not satisfy minimal requirements. Jets are called taggable if they fulfill the following requirements. Each jet is required to be matched, within a cone of  $\Delta R < 0.5$ , to a track-jet with  $\geq 2$  tracks. Track-jets begin with a seed-track of  $p_T > 1 \text{ GeV}$ , to which lower  $p_T$  tracks are added if they pass quality cuts and are within  $\Delta R < 0.5$  of the current track-jet direction and  $\Delta z < 2.0$  of the current track-jet  $z$  position. The track-jet direction and  $z$  position is updated upon the addition of each track. The track quality cuts require  $p_T > 1.0 \text{ GeV}$ ,  $\geq 1$  SMT hit, and the distance of closest approach to the primary vertex in the transverse and  $z$  directions to be less than 2 and 4 mm, respectively. The fraction of taggable jets is measured to be  $(76.5 \pm 2.7)\%$  per jet. This efficiency is a function of the  $|\eta|$  and the  $p_T$ , and is then applied to the simulated jets. After applying these selections, 2140 events remain in data.

### III. SIMULATED EVENT SAMPLE

The following processes are simulated to estimate the signal acceptance and the total number of expected background events:

- $ZH \rightarrow \nu\bar{\nu}b\bar{b}$  production generated by PYTHIA [6]
- $t\bar{t}$  production generated by PYTHIA
- The single top ( $t\bar{b}$  and  $tqb$  channels) generated by COMPHEP [7]
- $WZ \rightarrow l\nu jj$  and  $ZZ \rightarrow \nu\bar{\nu}b\bar{b}$  and  $\nu\bar{\nu}c\bar{c}$  production with ALPGEN [8],
- $W$ +jets events generated with ALPGEN including  $Wj$ ,  $Wjj$ ,  $Wcc$ , and  $Wcj$  process.  $W$  decays to  $e\nu, \mu\nu$ , and  $\tau\nu$ .
- $Z$ +jets events generated with ALPGEN including  $Zj$ ,  $Zjj$ ,  $Zcc$ , and  $Zcj$  process.  $Z$  decays to  $\nu\bar{\nu}$ ,  $ee, \mu\mu$ , and  $\tau\tau$ .
- $Wbb$  events generated by ALPGEN with  $W$  decays to  $e\nu, \mu\nu$ , and  $\tau\nu$ .
- $Zbb$  events generated by ALPGEN with  $Z$  decays to  $\nu\bar{\nu}$ ,  $ee, \mu\mu$ , and  $\tau\tau$ .

The samples generated by COMPHEP and ALPGEN are passed through PYTHIA showering and hadronization. The next to leading order cross section calculations given by MCFM are used [9],[10]. The branching ratios of  $W$  and  $Z$  decays are taken from PDG 2004 [11]. The instrumental background is measured in data, but are also simulated by PYTHIA in order to study variables used in the background estimation.

All the samples were processed through the  $D\bar{O}$  detector simulation (DØgstar [12], based on GEANT), the electronics simulation (DØsim), and the reconstruction software (DØreco). Trigger efficiencies, measured in data, were then applied to the simulated events.

### IV. INSTRUMENTAL BACKGROUND ESTIMATION

The remaining instrumental background is estimated from a fit to the  $\text{Asym}(\cancel{E}_T, \cancel{H}_T)$  distribution. The distributions of  $\text{Asym}(\cancel{E}_T, \cancel{H}_T)$  in the physics and instrumental backgrounds are estimated by the double gaussian function (FIG.3(a)) from simulation and by the exponential function from data in the sideband region (FIG.3(b)), respectively. The instrumental background simulation also confirms that the exponential function describes the data in both the signal and sideband regions. The fit results for the total number of physics and instrumental background

TABLE I: Number of expected signal and background events, and observed events in data before  $b$ -tag, after single  $b$ -tag, and double  $b$ -tag.

	$Z+\geq 2\text{jets}$	$Z+\geq 2\text{jets}$ with 1 $b$ -tag	$Z+\geq 2\text{jets}$ with 2 $b$ -tags
$ZH/WH$	0.62	0.4	0.1
$Zjj/Zbb$	525.3	23.9	2.1
$Wjj/Wbb$	1062.9	72.6	2.4
$t\bar{t}/tb/tqb$	9.7	5.0	0.8
$WZ/ZZ$	3.0	1.1	0.2
Instrumental background	524.2	42.1	0.9
Total expectation	2125.0	144.7	6.4
Observed event	2140	132	9

events are  $1579 \pm 65$  and  $524 \pm 57$ , respectively. From simulation, the number of physics backgrounds is expected to be  $1600 \pm 45$  events, which is in agreement with data. FIG.4 shows the  $\text{Asym}(\cancel{E}_T, \cancel{H}_T)$  for data in the signal region. A fit using a double gaussian and an exponential describes the data well. The physics background in the sideband, estimated by simulation, is subtracted from data in the sideband. The difference of the leading jet  $p_T$  between the signal and sideband data is corrected for. The level of the correction is  $\approx 10\%$ . The corrected data in the sideband is normalized to the expected number of instrumental background events from the fit, and are used for the estimation of the event yields after the  $b$ -tagging. FIG.5 shows the  $p_T$  of the first and second leading jets,  $\cancel{E}_T$ , and the invariant mass formed with the two leading jets. The data agree well with simulation, after accounting for the estimated instrumental background.

## V. $b$ -TAG RESULTS

The  $b$ -tagging algorithm uses a lifetime probability that is estimated from the tracks associated with a given jet. A small probability corresponds to jets having tracks with large impact parameters that characterize  $b$ -hadron decay. We cut on a lifetime probability smaller than 0.7%, which is known to give a mistag rate (tagging of light quarks) of  $(0.5 \pm 0.05)\%$ . The tagging efficiency for a “taggable” jet is measured to be  $(43 \pm 3)\%$ . For the simulated jets, we apply  $b$ -tag efficiency and charm and light quark tag rate functions, depending on the flavor of the jets. The type of the jets are determined by the simulated hadrons within  $\Delta R < 0.5$  of the jet axis. For the instrumental background, we estimate the total tag rate in the sideband regions, which is  $(4.2 \pm 0.6)\%$ .

TABLE I lists the number of Higgs, background, and observed events for each  $b$ -tag requirement. After the double  $b$ -tag requirement, 9 events remain, while 6.4 events are expected. The dominant background is  $W$  or  $Z$  + jets. FIG.6 shows the  $p_T$  of the first and second leading jets,  $\cancel{E}_T$ , and the invariant mass formed with the two leading jets, when at least one of the two leading jets passes the  $b$ -tagging requirement (single  $b$ -tag). FIG.7 shows the  $p_T$  of the first and second leading jets (double  $b$ -tag),  $\cancel{E}_T$ , and the invariant mass formed with the two leading jets, when both leading jets pass the  $b$ -tagging requirement.

## VI. $ZH$ CROSS SECTION LIMIT

We search for an excess of events in a dijet mass ( $M_{jj}$ ) window. The resolution of dijet mass is estimated to be 15 % by signal simulation. We apply  $80 \text{ GeV} < M_{jj} < 130 \text{ GeV}$  for  $M_H = 115 \text{ GeV}$ . After the mass cut, 3 events remain, while 2.2 backgrounds are expected.

We estimate the systematic uncertainty due to jet reconstruction efficiency, jet energy scale factor, jet resolution,  $b$ -tagging (including taggability), instrumental background estimation, and background cross section. The estimation is performed by varying each source of uncertainty by  $\pm 1 \sigma$  and repeating the analysis. TABLE II lists the systematics for each uncertainty. The total systematic error of signal acceptance and backgrounds are 26 % and 33 %, respectively. The uncertainty from luminosity is estimated to be 6.5 %.

With  $(0.33 \pm 0.08)\%$  signal acceptance (including  $B(Z \rightarrow \nu\bar{\nu}) = 20\%$ ),  $2.2 \pm 0.7$  events of expected background, and  $(261 \pm 17) \text{ pb}^{-1}$  of integrated luminosity, the limit on the cross section for  $\sigma(pp \rightarrow ZH) \times B(H \rightarrow b\bar{b})$  for  $M_H = 115 \text{ GeV}$  is 9.3 pb at the 95 % confidence level. The results for the other masses are listed in TABLE III and plotted in FIG. 8.

TABLE II: The systematic uncertainties and their sources. In addition to these errors, the uncertainty of the integrated luminosity is 6.5 %.

Source	Signal Acceptance (%)	Background (%)
Jet identification (5 % per jet)	7	6
Jet energy scale	7	8
Jet resolution ( $\sim 10$ %)	5	3
Taggability (4% per jet)	7	6
$b$ -tag ( $\sim 10$ %)	22	25
$b$ -tag for instrumental background(14 % per jet)	-	5
Instrumental background expectation(11 %)	-	2
Background cross section (20 %)	-	17
Total	26	33

TABLE III: Signal acceptance (including  $B(Z \rightarrow \nu\bar{\nu}) = 20\%$ ), number of expected background events, and limits on the the cross section for  $\sigma(p\bar{p} \rightarrow ZH) \times B(H \rightarrow b\bar{b})$  at 95 % C.L., for  $M_H = 105, 115, 125,$  and  $135$  GeV.

Higgs Mass	105 GeV	115 GeV	125 GeV	135 GeV
Mass window	70<M<120	80<M<130	90<M<140	100<M<150
Data	4	3	2	2
$ZH/WH$	0.11	0.082	0.060	0.034
( $ZH (H \rightarrow b\bar{b})$ channel Acceptance (%))	(0.29 $\pm$ 0.07)	(0.33 $\pm$ 0.08)	(0.35 $\pm$ 0.09)	(0.34 $\pm$ 0.09)
$Zjj/Zbb$	0.73	0.67	0.59	0.52
$Wjj/Wbb$	1.08	0.69	0.63	0.57
$tt/tb/tqb$	0.30	0.32	0.33	0.31
$WZ/ZZ$	0.19	0.13	0.07	0.03
Instrumental	0.45	0.37	0.32	0.28
TOTAL backgrounds	2.75 $\pm$ 0.88	2.19 $\pm$ 0.72	1.93 $\pm$ 0.66	1.71 $\pm$ 0.57
Limit of $\sigma(p\bar{p} \rightarrow ZH) \times Br(H \rightarrow b\bar{b})$ (pb)	12.2	9.3	7.7	8.5
Expected Limit (pb)	8.8	7.5	6.0	6.5

## VII. SUMMARY

We have performed a search on  $261 \text{ pb}^{-1}$  of data, for  $ZH$  associated production in the  $\nu\bar{\nu}b\bar{b}$  channel. We have studied the dijet mass spectrum of the two leading  $b$ -tagged jets for Higgs boson masses between 105 and 135 GeV. In the absence of signal, we have set 95 % C.L. upper limits between 7.7 to 12.2 pb on the cross section for  $ZH$  production multiplied by the branching ratio for  $H \rightarrow b\bar{b}$ . These limits on  $ZH$  production are comparable to the upper limits on  $WH$  production reported in 2004 [13], which were obtained with  $174 \text{ pb}^{-1}$  of integrated luminosity.

## Acknowledgments

We thank the staffs at Fermilab and collaborating institutions, and acknowledge support from the Department of Energy and National Science Foundation (USA), Commissariat à l'Énergie Atomique and CNRS/Institut National de Physique Nucléaire et de Physique des Particules (France), Ministry for Science and Technology and Ministry for Atomic Energy (Russia), CAPES, CNPq and FAPERJ (Brazil), Departments of Atomic Energy and Science and Education (India), Colciencias (Colombia), CONACyT (Mexico), Ministry of Education and KOSEF (Korea), CONICET and UBACyT (Argentina), The Foundation for Fundamental Research on Matter (The Netherlands), PPARC (United Kingdom), Ministry of Education (Czech Republic), Natural Sciences and Engineering Research Council and West-Grid Project (Canada), BMBF (Germany), A.P. Sloan Foundation, Civilian Research and Development Foundation, Research Corporation, Texas Advanced Research Program, and the Alexander von Humboldt Foundation.

[1] Report of the Tevatron Higgs Working Group, hep-ph/0010338

[2] Results of the Tevatron Higgs Sensitivity Study, FERMILAB-PUB-03/320-E

[3] M. L. Ciccolini, S. Dittmaier, M. Krame, Phys. Rev. D68 (2003) 073003

- [4] V. Abazov, et al., in preparation for submission to Nucl. Instrum. Methods Phys. Res. A, and T. LeCompte and H.T. Diehl, “The CDF and DØUpgrades for Run II”, Ann. Rev. Nucl. Part. Sci. **50**, 71 (2000).
- [5] S. Abachi, *et al.*, Nucl. Instrum. Methods Phys. Res. A **338**, 185 (1994).
- [6] T. Sjostrand, P. Eden, C. Friberg, L. Lonnblad, G. Miu, S. Mrenna and E. Norrbin, “High-energy-physics event generation with PYTHIA,” Comput. Phys. Commun. **135**, (2001) 238
- [7] A. Pukhov *et al.*, COMPHEP, hep-ph/9908288 (1999)
- [8] M. Mangano et al.: ALPGEN, a generator for hard multiparton processes in hadron collisions, JHEP 0307 001 2003, hep-ph/0206293
- [9] John Campbell and R.K. Ellis, Phys. Rev. D65:113007 (2002), hep-ph/0202176.,
- [10] John Campbell and R.K. Ellis, ”MCFM - Monte Carlo for FeMtobarn processes”, <http://mcfm.fnal.gov/>
- [11] S. Eidelman et al., Phys. Lett. B592, 1 (2004)
- [12] Y. Fisyak and J. Womersley, DØ-Note 3191
- [13] DØ Collaboration, A Search for  $Wb\bar{b}$  and  $WH$  Production in  $p\bar{p}$  Collisions at  $\sqrt{s}=1.96$  TeV, hep-ex/0410062, Phys. Rev. Lett. **94**, 091802 (2005)

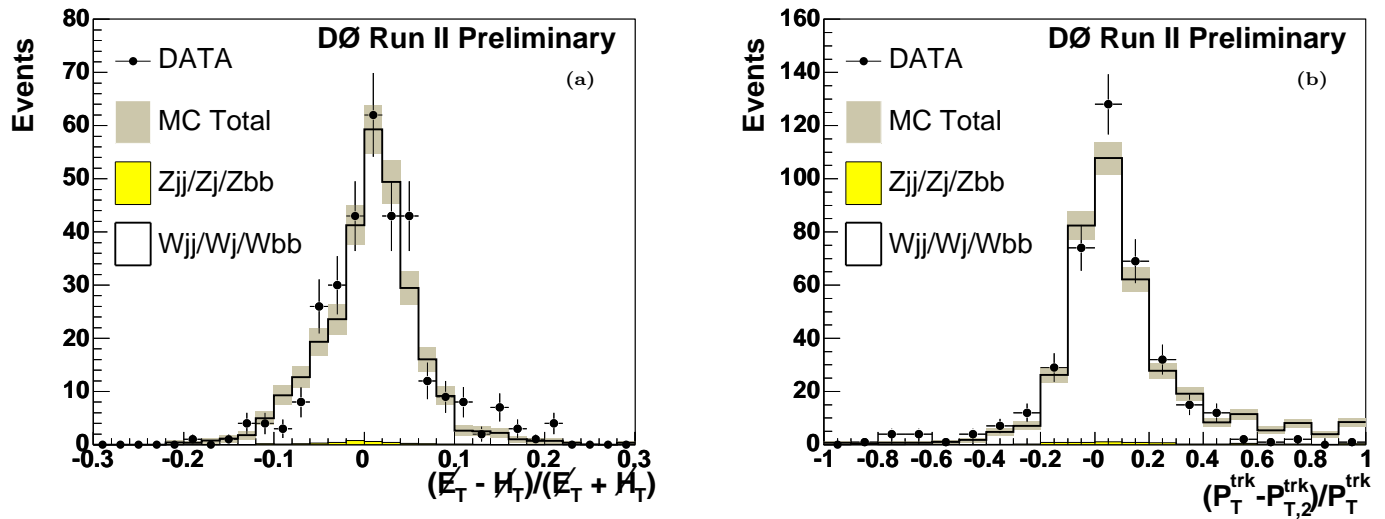


FIG. 1: (a) : Distribution of  $\text{Asym}(\cancel{E}_T, \cancel{H}_T)$  and (b) :  $R_{P_T^{\text{trk}}}$  distributions for the  $W$ + jets sample. Hatched bars show the statistical error of the simulation. For both distributions, the simulation and data agree well.

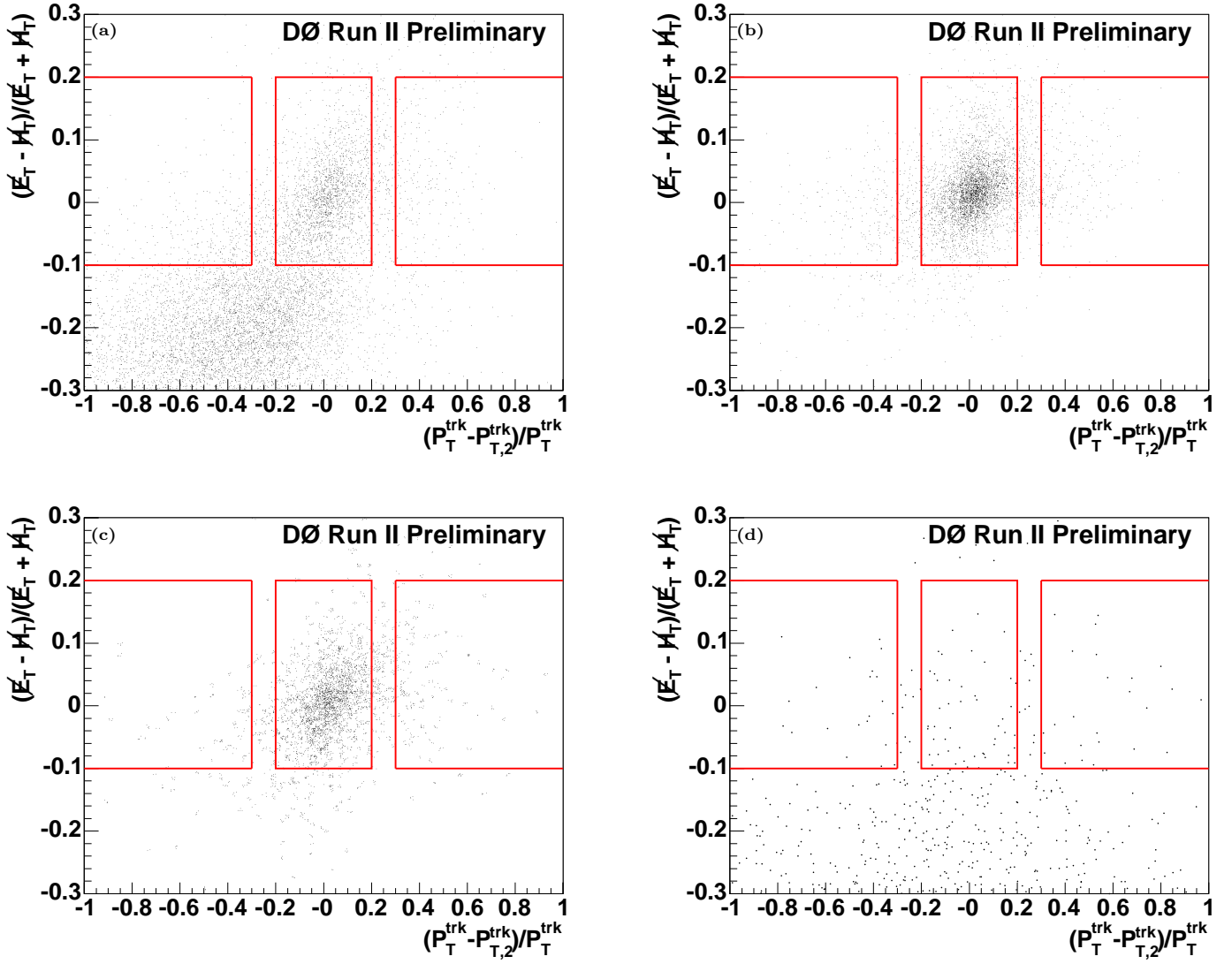


FIG. 2: Scatter plot of the  $\text{Asym}(\cancel{E}_T, \cancel{H}_T)$  and  $R_{P_T^{\text{trk}}}$ . (a) Data, (b) signal simulation, (c) physics background simulation, and (d) instrumental background simulation. The center box shows the signal region and the left and right boxes show the sideband region.

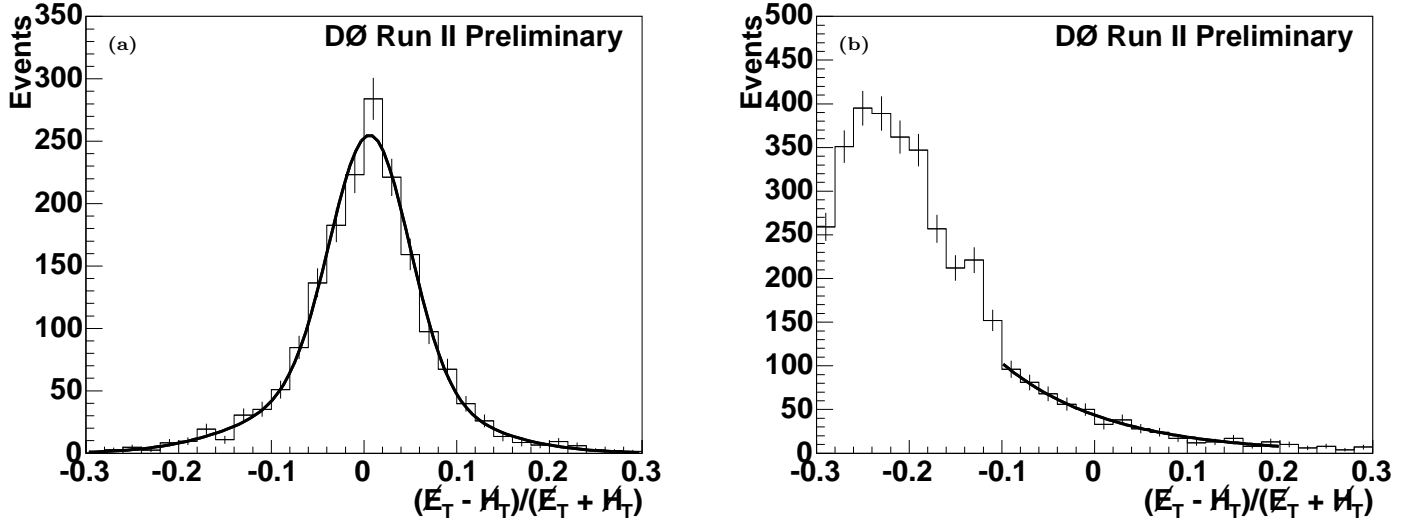


FIG. 3:  $\text{Asym}(E_T, \cancel{H}_T)$  for physics background estimated with simulation (a) and instrumental background estimated with sideband data (b). The physics background is modeled by a double gaussian fit and instrumental background is modeled by an exponential fit. These functions are used for a fit of the data in the signal region (FIG.4).

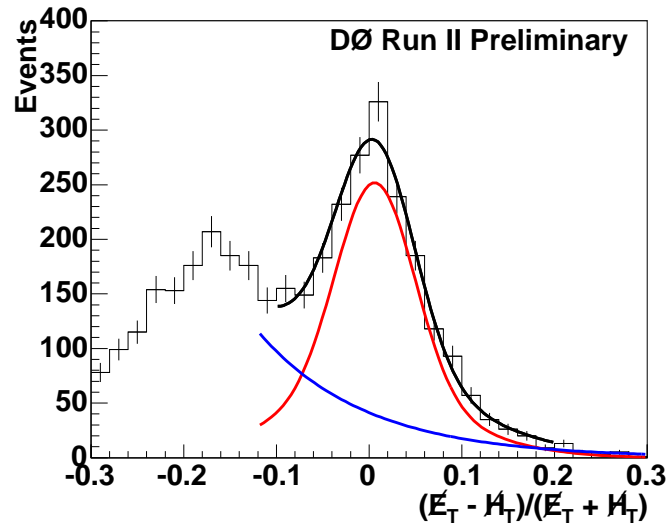


FIG. 4:  $\text{Asym}(E_T, \cancel{H}_T)$  for data in the signal region. A fit of double gaussian + exponential describe the data well. From the fit,  $1579.7 \pm 65.0$  physics backgrounds and  $524.2 \pm 57.2$  instrumental backgrounds are expected.

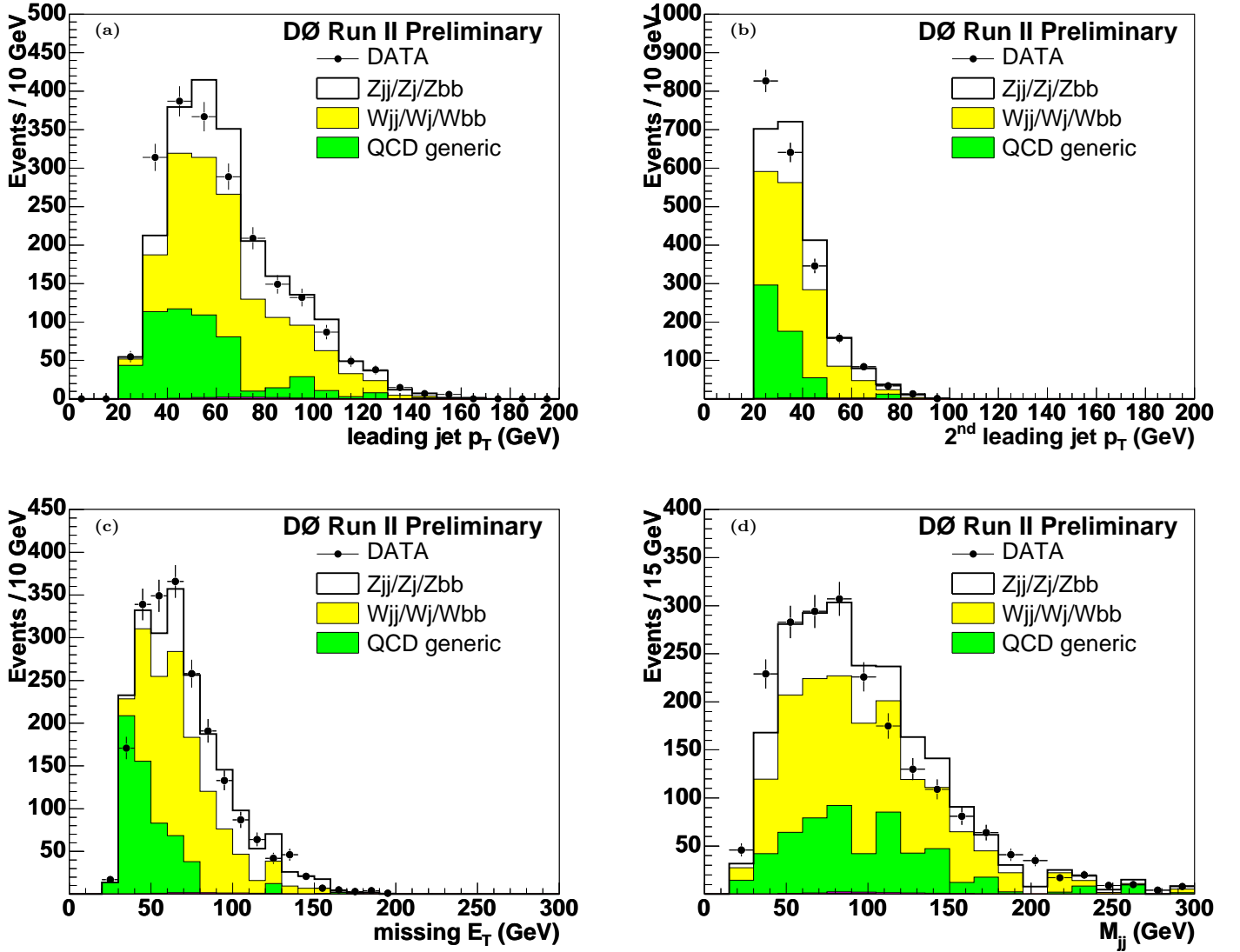


FIG. 5: The distributions after all selections except for  $b$ -tag. After accounting for instrumental background, the data agree well with simulation. (a)  $p_T$  of the leading jet, (b)  $p_T$  of the second leading jet, (c)  $\cancel{E}_T$ , and (d) invariant mass of two leading jets.

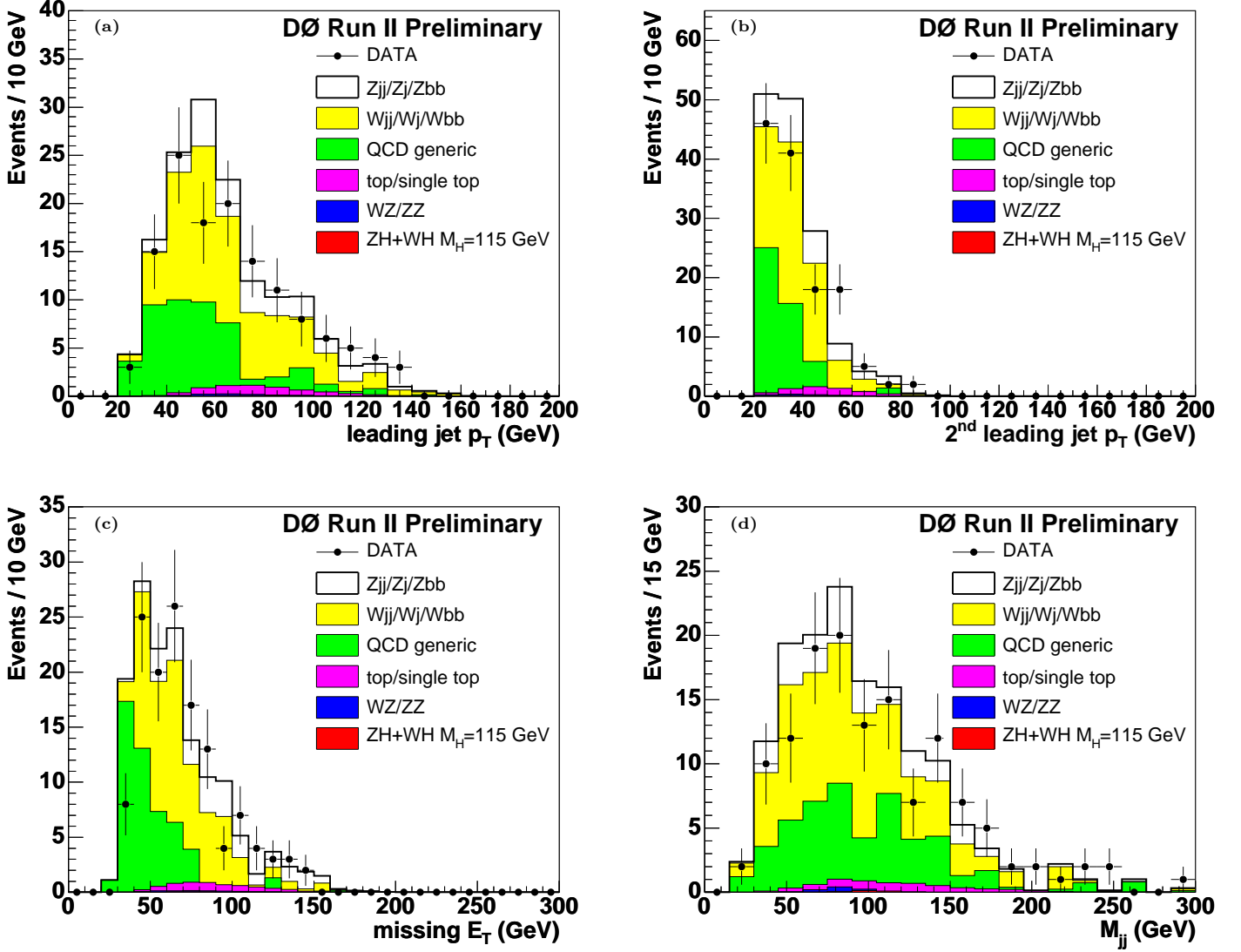


FIG. 6: The distributions after single  $b$ -tag. Simulation describes data well, which indicates that the  $b$ -tag performance is understood well. (a)  $p_T$  of the leading jet, (b)  $p_T$  of the second leading jet, (c)  $\cancel{E}_T$ , and (d) invariant mass of the two leading jets.

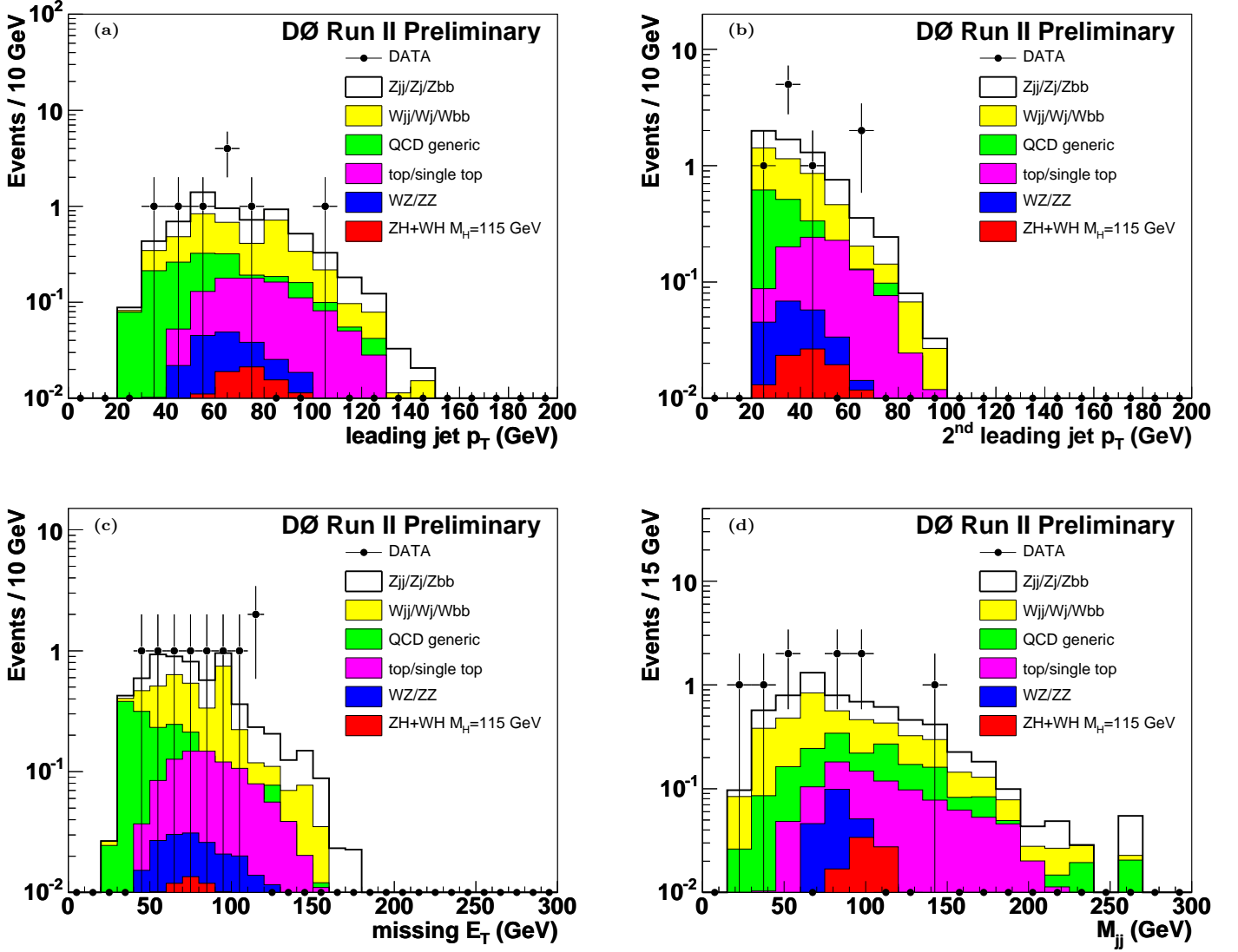


FIG. 7: The distributions after double  $b$ -tag in log scale. (a)  $p_T$  of the leading jet, (b)  $p_T$  of the second leading jet, (c)  $\cancel{E}_T$ , and (d) invariant mass of the two leading jets.

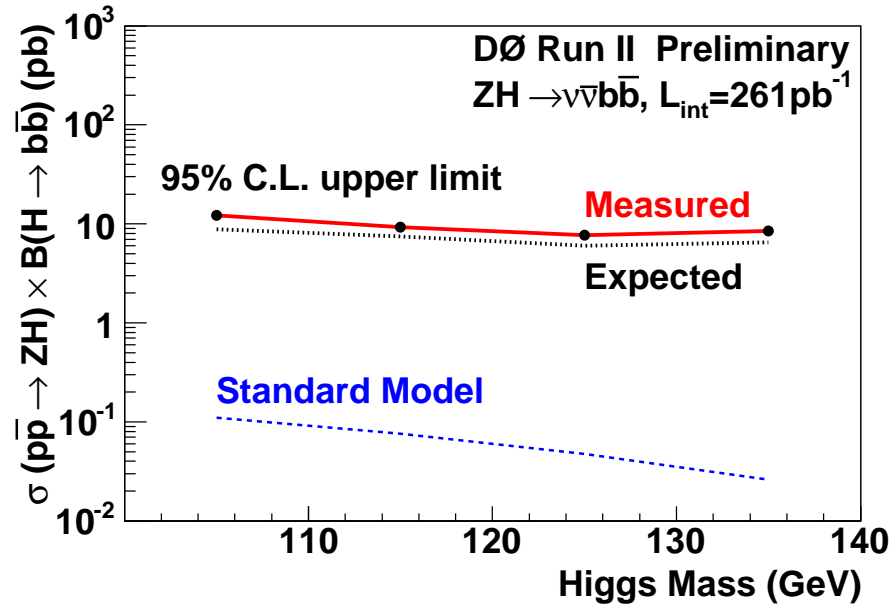


FIG. 8: 95 % C.L. upper limits on the cross section for  $ZH$  production times the branching ratio for  $H \rightarrow b\bar{b}$ .